Lab on a Chip

Cite this: *Lab Chip*, 2011, **11**, 4187

www.rsc.org/loc

PAPER

High-resolution cantilever biosensor resonating at air–liquid in a microchannel

Jungwook Park,*[a] Shuhei Nishida,[a] Pierre Lambert,[b] Hideki Kawakatsu[a] and Hiroyuki Fujita[a]

Received 7th July 2011, Accepted 30th August 2011
DOI: 10.1039/c1lc20608g

We have developed a highly mass-sensitive cantilever resonating at the interface of air and liquid. The cantilever is applicable as a biosensor by measuring its resonance frequency shift associated with the selective trapping of target molecules. One surface of the cantilever facing to the liquid is functionalized for label-free detection, while the opposite side is exposed to air to improve the resonance characteristics, such as the quality factor. The quality factor at resonance is 15, which is 50% higher than the same cantilever in liquid. The beam was excited through the photothermal effect of a power modulated laser and detected by laser Doppler velocimetry. Due to the proposed configuration, the signal-to-noise-ratio is 5.7 times larger than the completely submerged case. A micro-slit around the cantilever separates the air and liquid phases at a meniscus. We analyzed the cantilever motion including the meniscus membrane, and examined the effect of surface tension by applying various solutions. A slit width of 6 μm was found to give the best performance within the few prototypes. We measured the covalent immobilization of antibody molecules on a cantilever surface for three different concentrations: 20, 40, and 80 μg ml^{-1}. The kinetics measured by both resonance frequency shift of the cantilever and fluorescent intensity showed good agreement.

1. Introduction

Lab-on-a-chip has been contributing to biology and pharmaceutical development with superior functionality and fast reaction times of minutes or even seconds.[1–3] However, detection methods mainly depend on optical means; this results in the need for expensive fluorescent-regents, laborious molecular labeling and difficulty in continuous monitoring for extended periods.[4] Surface Plasmon Resonance (SPR) and quartz crystal microbalance (QCM) are two of the candidates commercially available as alternatives to the typical optical method. However, these techniques are not easily adapted to miniaturization and batch fabrication.[5,6]

The microcantilever has attracted much attention as a biosensor for its high sensitivity and simple structure. Its sensing principles are generally categorized into two kinds: static-mode, and dynamic-mode mechanical biosensor. In static-mode, one side of the cantilever should be functionalized to detect specific biomolecules. As the biomolecules bind, surface stress induces a deflection that is measured by the reflection of a laser beam onto a photodiodes array.[7–9]

In dynamic-mode, the resonance frequency shift indicates the mass of target molecules loaded on the functionalized surface. Although it has high sensitivity in air, researchers have had difficulty applying it to bio-applications because the bioreaction occurs in liquid which makes the vibration peak much less pronounced to hydrodynamic loading. In this regard, alternative operating environments have been studied, such as a humid environment, and molecular capture in liquid and detection in air. Real-time measurement of growth of bacterial colonies was achieved in a humid environment.[10,11] A cantilever is functionalized for label-free attachment of targets in liquid and detection is carried out in air. Recently prostate-specific antigen (PSA) in serum at femto-molar concentration was detected, but unidentified molecules may attach to the device and antibodies can deform during desiccation causing error of measurement.[12,13] The dynamic-mode cantilever resonating in liquid has promise to achieve continuous monitoring of bioreactions. However in highly viscous environments, its resonance property is limited by a low quality factor that is closely related to sensitivity and mass resolution.[14,15] Therefore, the technique was limited to detect bacterial virus T5.[16] To improve its resonance characteristic in liquid, higher resonance modes such as 1st and 2nd torsion mode have been studied.[17,18] As an alternative approach to cantilever biosensing, a suspended microchannel resonator (SMR) has been devised by embedding a microchannel in the beam. The resonator showed high-resolution resonance frequency with a noise level below 27 ag (10^{-18} g) with a 1 Hz bandwidth.[19] SMR achieved not only label-free detection in the embedded

[a]*Center for International Research on Micronano Mechatronics (CIRMM), Institute of Industrial Science (IIS), the University of Tokyo, 4-6-1 Komaba Meguro, Tokyo, 153-8505, Japan. E-mail: jwook@iis.u-tokyo.ac.jp; Fax: +81 3 5452 6250; Tel: +81 3 5452 6248*
[b]*Laboratory of Integrated Micro and Mechatronics Systems/CNRS-IIS, UMI 2820, 4-6-1 Komaba Meguro, Tokyo, 153-8505, Japan. E-mail: Pierre.lambert@ulb.ac.be*

microchannel, but also measurements of the mass growth rate of buoyant individual cells and nano-particles with a centrifugal or passing through mode.[20–23] But the resonator should be placed in a vacuum chamber, and the device is fragile to high liquid pressures so that liquid must be induced through a bypass channel.[24]

In this paper, we demonstrate a new method based on a cantilever resonating at air–liquid for high-resolution detection of biomolecules in a microchannel. The structure has the advantages of better resonance characteristics and lower noise levels in a readout signal, compared to a cantilever resonating in liquid. However, in addition to the mass loading on the cantilever, the resonance frequency of the novel resonator is susceptible to the surface tension at the micro-slit and liquid pressure changes in the channel. Here, we analyzed and examined those effects with theoretical calculations and empirical methods to solve those problems. In the end, we confirmed the sensitivity and continuous monitoring capability of the cantilever biosensor by observing covalent attachment of antibodies to a cantilever surface. For three concentrations of 20, 40, and 80 μg ml^{-1}, resonance frequency shift and fluorescent intensity change were compared and showed good agreement.

2. Cantilever at air–liquid interface

2.1. Device configuration

The cantilever is cut out of the bottom of a microchannel and is defined by the surrounding micro-slit (Fig. 1(b, c)). One surface of the cantilever faces the liquid layer and is functionalized for label-free detection of biomolecules, while the opposite side is exposed to air to improve the resonance characteristics including higher quality factor and larger vibrating amplitude. The micro-slit around the cantilever splits air–liquid phases at a meniscus membrane formed by a surface tension.

2.2. Principle to sustain liquid by micro-slit

The meniscus membrane at the micro-slit has a role to maintain liquid pressure in the microchannel: its initial shape was assumed to be totally flat. Under the effect of a pressure gap Δp between the liquid and the air, this shape was deformed, assuming that the interface shape had one of its curvature radius infinite (zero curvature), while the second curvature radius was r (see detail G-G of Fig. 2). The Laplace equation gives the relationship between Δp and r:

$$\Delta p = \frac{\gamma}{r} \tag{1}$$

while r can be related through simple geometrical relationship to the slit s:

$$2r \sin t = s \tag{2}$$

hence the pressure gap is given by:

$$\Delta p = \frac{2\gamma \sin t}{s} \tag{3}$$

The pressure gap Δp is however limited either by the condition $t = \frac{\pi}{2}$ or by a smaller angle t if the advancing contact angle made by the liquid on the cantilever is smaller than $\frac{\pi}{2}$. We see that the smaller the slit s, the larger the pressure the interface can balance.

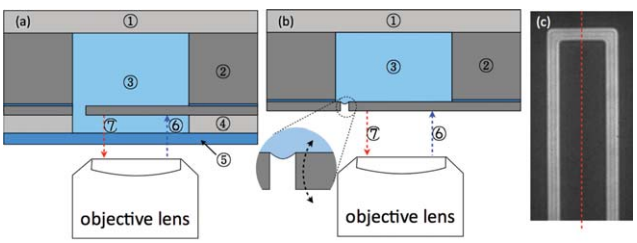

Fig. 1 Comparison of cantilevers integrated in the microchannel: (a) Cantilever resonating in the microchannel (③) covered by a PDMS sheet (①) and a glass plate (⑤) with a PDMS spacer (④). The cantilever is made out of a silicon-on-insulator substrate (②). (b) Cantilever resonating at air–liquid on the bottom of the microchannel to improve the resonance characteristics and signal-to-noise-ratio. (c) Microscopic view of the cantilever shown in (b), the optical fringe patterns in the meniscus are observed along the micro-slit that defines the cantilever. The vibration is excited through the photothermal effect of a pulsed laser beam (⑥) and detected by another beam (⑦) for laser Doppler velocimetry.

2.3. Fabrication process

The dimensions of the cantilever were 80 μm × 20 μm × 5 μm for all the experiments. The widths of the micro-slit were varied (4, 6, and 10 μm) to examine the effect of the meniscus formed at the slit. The size of microchannel was 100 μm (w) × 400 μm (h) × 10 mm (l), as illustrated in Fig. 3(a). The device was fabricated using a silicon-on-insulator (SOI, 5 μm (Si)/1 μm (SiO_2)/450 μm (Si), Ultrasil) wafer to obtain a uniform thickness over the cantilever area.

First, the wafer was cleaned with piranha solution, a mixture of sulfuric acid and hydrogen peroxide in the ratio of three to one, at 150 °C on a hot plate. Next, buffered hydrofluoric (BHF) acid removed the natural oxide in 30 s. An aluminium (Al) layer was deposited and patterned on the backside of the SOI wafer as a metal mask for defining the microchannel. The 5 μm thick silicon layer was then patterned by the Deep Reactive Ion Etching (DRIE) process. The fabricated cantilever was protected by a painted photoresistor (S1818). The thick silicon layer was dry-etched with the DRIE process from the backside. The buried

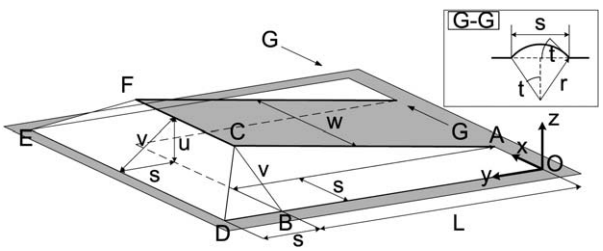

Fig. 2 Sketch of the cantilever (length L and width w), a slit of width s and a gas–liquid interface, made of a trapezoidal shape $CDEF$, two triangles BCD and two lateral areas $OACB$. The cantilever tip deflection, u, is assumed to be smaller than s and L. G-G: sketch of a deformed air–liquid interface along the slit: one of the curvatures is equal to zero, while the second one is equal to $1/r$.

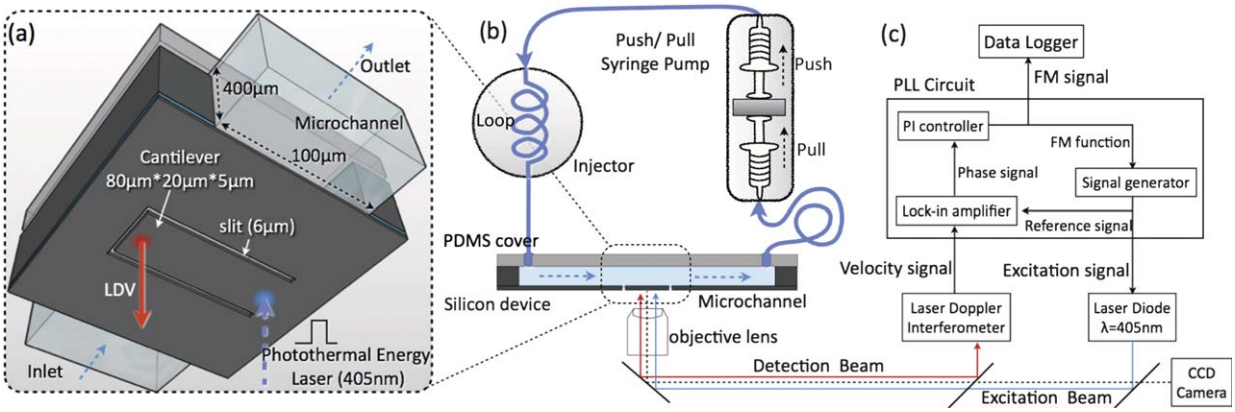

Fig. 3 Experimental setup for the cantilever biosensor with a closed microfluidic circuit and an excitation system controlled by a closed feedback loop: (a) schematic representation of the cantilever in the microchannel, (b) the closed fluidic system to stabilize the liquid pressure in the microchannel by the push/pull syringe pump and balanced fluidic resistances between the pump and the chip. (c) Vibration of the cantilever is measured by laser Doppler velocimetry while it is excited by a photothermal laser. The resonance peak is tracked by keeping the phase difference between excitation and vibration signals constant. The feedback system is composed of a lock-in amplifier, a PI controller and a programmable signal generator.

silicon dioxide layer was removed with an 8-minute BHF etching. Finally, an approximately 130 nm-thick silicon dioxide layer was sputtered from the backside onto the cantilever surface facing the microchannel to have the hydrophilic surface for bio-affinity.

We covered the microchannel using a commercially available 2 mm thick PDMS sheet to allow an inlet and outlet to link the polytetrafluoroethylene (PTFE) tube (0.7/0.3, outer/inner diameter).

2.4. Excitation and measurement system with two lasers

An efficient photothermal laser is used to actuate the resonator.[25,26] The photothermal laser (λ = 405 nm) intermittently heats the fixed-end resulting in a vibrating amplitude that was measured at the free-end of the cantilever by laser Doppler velocimetry (LDV, λ = 633 nm). As shown in Fig. 3(c), the measurement system consists of four parts; a laser Doppler velocimetry, a photothermal laser, a closed-loop feedback control to track the resonance frequency, and a plate that can be adjusted in x-axis and y-axis directions. The environment change affects the resonance frequency of a cantilever. Therefore, it should be controlled during the experiment for precise measurement. All the liquids were kept at the same temperature; this stabilized the temperature of the cantilever. We also used an anti-vibration table to eliminate the mechanical disturbance from the environment.

The velocity signal detected by the LDV was fed back to a lock-in-amplifier to compare the LDV signal and the photothermal laser signal. The frequency data was converted to a voltage corresponding to the output of the sensor. A proportional-integral (PI) controller compensated the phase difference between excitation and vibration signals. The resonance frequency was stored in a data-logger programmed in LabVIEW.

2.5. Result for resonance frequency characteristics

The cantilever resonating at air–liquid has advantages of not only higher vibrating amplitude and better quality factor, but also less noise due to removal of air/glass/liquid interfaces that scatter the detection laser beam. We characterized the novel cantilever resonating at the interface and compared it with the cantilever in liquid. The resonance characteristic was measured with a resolution of 100 Hz using a network analyzer (E5071C, Agilent technologies), by sweeping a frequency in the range of $\pm$150 kHz with a reference power of -6 dBm.

Fig. 4 shows the resonance characteristics of cantilevers at an air–liquid interface (shown in Fig. 4(b)) and in liquid (a). The cantilever at the interface has a resonance peak at 919.5 kHz, a quality factor of 15 and an amplitude of 170 pm (10^{-12}) with exciting laser power of 2 mW, while the same cantilever in air has a resonance peak at 1191 kHz. It also had less noise on its amplitude and phase in Fig. 4(b) than the fully submerged case. On the other hand, when the cantilever was immersed in the purified water, the vibrating amplitude decreased to 110 pm at a resonance peak of 788.5 kHz and quality factor of 10 (Fig. 4(a)). Fig. 4(c) compares the amplitudes in the two environments. The amplitude in Fig. 4(b) is 62% larger and shows a 50% better quality factor than the peak in Fig. 4(a). Fig. 4(d) shows a comparison of the noise level in the phase component of the cantilever motion. The data was subtracted from phase signals using a moving average of 21 adjacent points. The phase signal in Fig. 4(b) shows a 5.7-fold increase in signal-to-noise-ratio compared to in Fig. 4(a). In this respect, a cantilever at an air–liquid interface achieves 25 times higher frequency resolution than one in liquid, which corresponds to a mass resolution of 10^{-16} g, based on eqn (3) in ref. 27.

3. Surface tension on the micro-slit

3.1. Effect of the meniscus elastic membrane

The effect of surface tension is to resist against stretching of air–liquid interface: if the cantilever undergoes a tip deflection u, the area A increases, leading to an increase of the surface energy $W = \gamma A$, where γ is the surface tension of the liquid. It will be shown in the following that W can be written in the form:

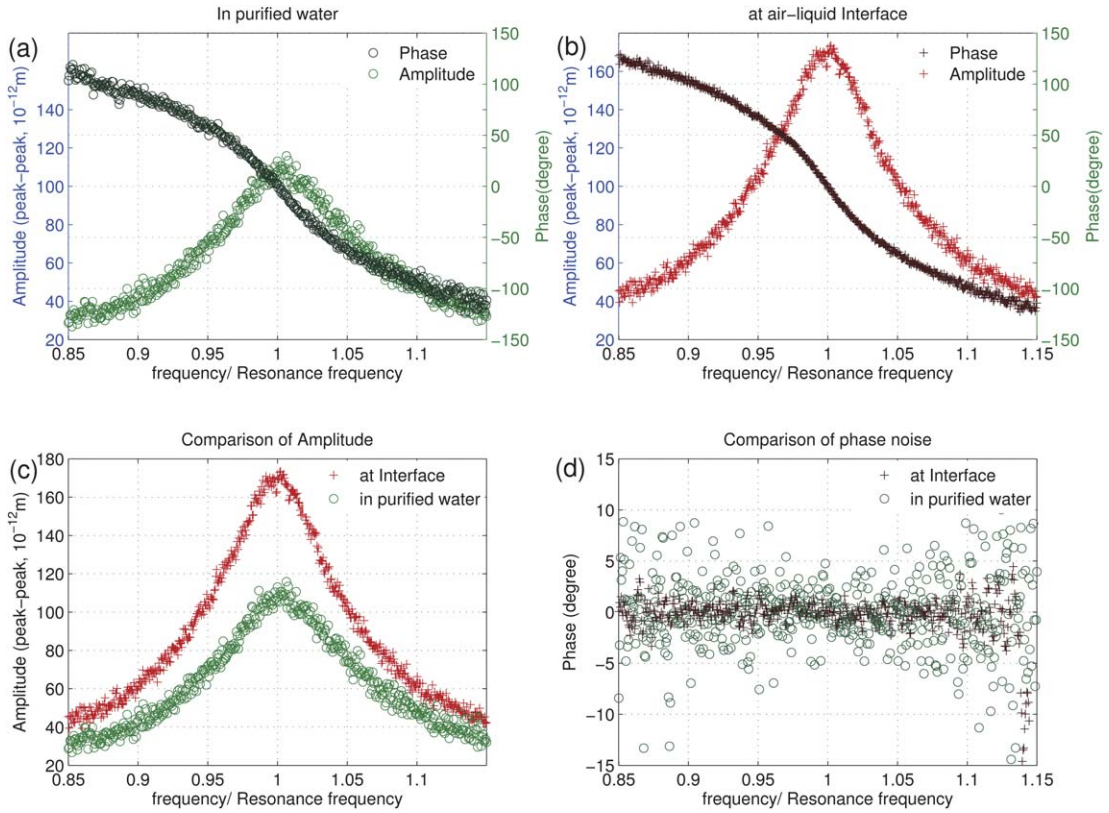

Fig. 4 Resonance frequency characteristics of cantilevers in liquid (a) and resonating at air–liquid (b); (a) cantilever in liquid: quality factor of 10 with larger noise present in signal, (b) cantilever at the interface: quality factor of 15 with less noise; (c) comparison of amplitude between (a) and (b): (b) has 62% higher amplitude and 50% higher quality factor than (a); (d) noise level comparison on phase signal: (b) has a 5.7-fold increase in signal-to-noise-ratio compared to (a).

$$W = W_{\text{constant}} + \frac{1}{2}ku^2 \tag{4}$$

Eqn (5) means the membrane works as a spring. Air–liquid can be approximated as depicted in Fig. 2, including the front trapezoidal shape *CDEF*, two times the triangle *BCD* and two times the lateral area *OACB*, the latter being shown with more detail in Fig. 2. The geometry depicted in Fig. 2 is only an approximation, for two reasons: (1) the cantilever does not bend linearly; (2) the air–liquid interface must respect the so-called Laplace equation, *i.e.* present a constant curvature if the pressure is assumed to be constant in the liquid side of the interface. Obviously, this condition is not respected by the proposed geometrical shapes (1 trapeze + 2 triangles + 2 lateral areas), but the proposed model can at least determine the order of magnitude of the effect of surface tension.[28] Let us now compute the area of the three geometries, with the assumption that $u \ll s \ll L$:

1. Trapezoidal shape *CDEF*:

$$\begin{aligned} A_{\text{I}} &= \frac{(||ED|| + ||CF||)v}{2} \\ &= (w+s)s\sqrt{1+\left(\frac{u}{s}\right)^2} \\ &\approx (w+s)s\left(1+\frac{1}{2}\frac{u^2}{s^2}\right) \end{aligned} \tag{5}$$

2. Two times the triangular shape *BCD*:

$$\begin{aligned} A_{\text{II}} &= 2\frac{||DB|| \cdot ||BC||}{2} \\ &= s \cdot v \\ &\approx s^2\left(1+\frac{1}{2}\frac{u^2}{s^2}\right) \end{aligned} \tag{6}$$

3. Two times the lateral area *OACB* shown in Fig. 2:The z-coordinate of P' is equal to $z(P') = u\frac{x}{s}$, leading to the z-coordinate of an arbitrary point P:

$$z(P) = xy\frac{u}{sL} = xyQ \tag{7}$$

with $Q = \frac{u}{sL}$.

Now, the surface element of the lateral area *OACB* can be expressed as:

$$\begin{aligned} \mathrm{d}S &= \sqrt{1+\left(\frac{\partial z}{\partial x}\right)^2+\left(\frac{\partial z}{\partial y}\right)^2}\,\mathrm{d}x\mathrm{d}y \\ &= \sqrt{1+Q^2(x^2+y^2)}\,\mathrm{d}x\mathrm{d}y \\ &\approx \left(1+\frac{1}{2}Q^2x^2+\frac{1}{2}Q^2y^2\right)\mathrm{d}x\mathrm{d}y \end{aligned} \tag{8}$$

and the area of both lateral interfaces can be written as:

$$A_{III} = 2\int_0^s \int_0^L dS \approx 2\left[Ls + \frac{u^2}{6sL}(s^2 + L^2)\right] \quad (9)$$

Summing up $A = A_I + A_{II} + A_{III}$ and multiplying by surface tension γ to get the surface energy, we find:

$$W = \underbrace{\gamma(ws + 2s^2 + 2sL)}_{W_{constant}} + \underbrace{\frac{1}{2}u^2\gamma\left(2 + \frac{w}{s} + \frac{2}{3}\frac{s^2 + L^2}{sL}\right)}_{k} \quad (10)$$

which means that the smaller-width slit has a larger spring constant caused by the surface tension.

3.2. Effect of surface tension on resonance frequency

We have examined elastic properties of the meniscus membrane by changing the width of the micro-slit as well as a coefficient of the surface tension of the liquid. First, we fabricated the micro-slits of 4, 6, and 10 μm defining the cantilevers in the same microchannel. The dimensions of the cantilever were always kept constant. We prepared silicon cantilevers with a hydrophobic surface, in order to exclude any loaded mass on the cantilever. The microchannel was filled with purified water. Then, the resonance frequency of the cantilevers with various slit widths was measured one by one.

The cantilevers with micro-slit widths of 4, 6, and 10 μm had resonance frequencies of 741.0, 659.7, and 642.2 kHz, respectively. In terms of quality factor, the cantilever with a micro-slit width of 4 μm had a factor of 7, and the cantilevers with micro-slit widths of 6 μm and 10 μm had quality factors of 15 and 10, respectively. As a result, the cantilever with a micro-slit width of 6 μm has the largest quality factor, as shown in Fig. 5(a). But the reason is not known yet.

Next, we examined the effect of the surface tension coefficient of the liquid on the resonance frequency by applying poly-oxyalkylene sorbitan laurate (tween20) diluted in purified water, 0, 10^{-5}, 5×10^{-5} and 10^{-4} M (mol l^{-1}) as a positive control. And we prepared potassium chloride (KCl) solutions of 10^{-3}, 10^{-4}, 10^{-5} M concentrations as a negative control. The surface tension was measured by a goniometer (FAMAS, Kyowa interface measurement) with the pendant drop method.

The resonance frequency of the cantilever was correlated to the surface tension coefficient of solutions. The tween20 solution of 10^{-4} M, the most dense concentration, had a surface tension of 53 mN m^{-1}, and resulted in a resonance frequency shift of 1.57 kHz, while the cantilever had a resonance frequency shift of 0.95 and 0.01 kHz in tween20 of 5×10^{-5} and 10^{-5} M whose surface tensions were 57 and 67 mN m^{-1}, respectively, as shown in Fig. 5(b). In the negative control experiment, the resonance frequency was not shifted by any of the KCl solutions whose surface tension did not change depending on concentration. To sum up, the resonance frequency is correlated to the surface tension in tween20 solutions. However, changes in resonance frequency induced by a surface tension can be neglected because the resonance frequency shift was less than 0.27 kHz for the surface tension in the range from 60 to 72 mN m^{-1}. Moreover, the resonance frequency decreased more than the theoretical prediction because concentrated tween20 is more viscous than purified water which affected the resonance frequency of the cantilever in liquid.

4. Liquid pressure in the microchannel

4.1. Closed fluidic system to stabilize liquid pressure in the microchannel

The resonance frequency of the cantilever at the air–liquid interface is susceptible to the liquid pressure that introduces additional stress distribution along the thickness direction. To counter this, we have developed a closed fluidic system to stabilize the liquid pressure.

In this respect, the fluidic system was optimized to stabilize liquid pressure at the centre of the microchannel where the cantilever is placed. First, a push/pull type syringe pump (KD Scientific, KD270) was employed to push the flow to the inlet and to pull out the flow from the outlet at the same flow rate, as illustrated in Fig. 3(b). Second, the fluidic resistance of the tubes linking the pump and the inlet/outlet was balanced to apply

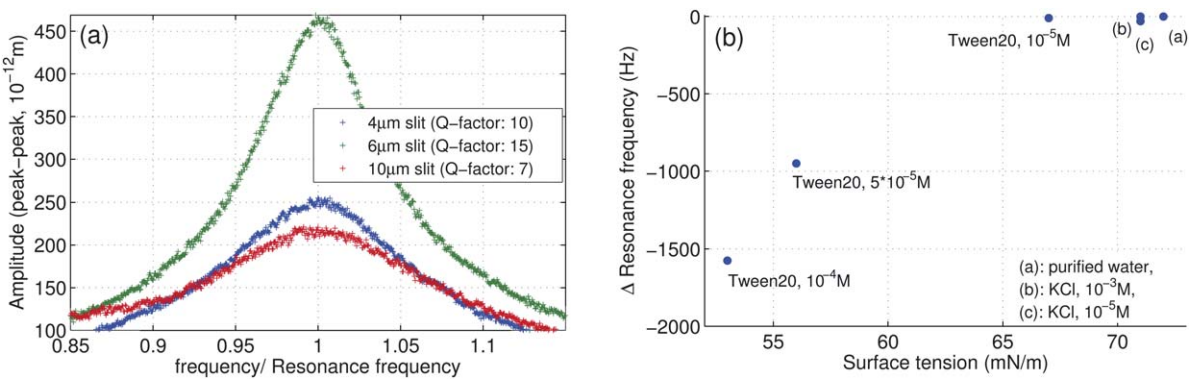

Fig. 5 Resonance frequency characteristics of cantilevers with various widths of the micro-slit (a), and surface tension changes (b). The graph shows the vibrating amplitude at the resonance peak as a ratio of frequency. The narrower gap has a higher resonance frequency and the cantilever with a 6 μm wide micro-slit has a higher quality factor than the rest (a). In (b), the resonance frequency could be decreased with various surface tension coefficients by the application of a tween20 surfactant. KCl was used as a negative control.

virtually zero liquid pressure in the centre of a microchannel. Third, a PTFE tube (Chukoh, AWG-30) was used to reduce the fluidic resistance. Finally, an injector (Upchurch scientific, V-451) was placed in between the syringe pump and the inlet of the microchannel for injecting different fluids. Using this improved closed fluidic system, the resonance frequency could be stabilized for as long as 2-hour measurements under the conditions of flow rate change.

5. Confirmation of biosensing capability

5.1. Sample preparation

The surface of the cantilever was functionalized with fluorescently-labeled antibodies and resonance frequency shifts as well as the change in fluorescent intensity were measured continuously. We used peptide bonding enhanced by EDC (1-ethyl-3-(3-dimethylaminopropyl)carbodiimide, (Bangs Laboratories Inc)) to bind between the carboxyl-group of antibodies and the free amino group on the cantilever previously coated with APTES (3-aminopropyltriethoxysilane, Dow Corning, 99%).

The cantilever was cleaned and activated by dipping in a piranha solution for 10 min. Then, the amino group was deposited on the silicon dioxide layer on the cantilever by applying APTES solution (5% APTES, 5% purified water, and 90% ethanol) for 30 min.[29] 2 mg ml^{-1} of EDC in its coupling buffer (0.5 mM of MES and 0.05% proclin300 at pH 5.2) was mixed in as a catalyst. Fluorescent antibodies (labelled rabbit anti-mouse IgG antibodies, Molecular Probes) of 20, 40, and 80 μg ml^{-1} concentration were prepared in EDC coupling solution just before the reaction.

5.2. Result for measurement of antibodies bonded on the cantilever

We measured a resonance frequency shift during the attachment process of fluorescent antibodies of various concentrations on the surface of the cantilever. We verified the results by a method of fluorescent microscopic observation.

We applied an EDC solution of 2 mg ml^{-1} after filling the microchannel with purified water at a flow rate of 3 μl min^{-1} using a closed fluidic system. Then, the fluorescent antibodies at a concentration of 20 μg ml^{-1} in EDC solution were introduced at a flow rate of 45 μl h^{-1} for one hour. The resonance frequency of the cantilever was measured by LDV while the photothermal laser excited the cantilever. The data was sampled at 10 Hz, low pass filtered with a cut off frequency of 1 kHz with sensitivity of 30 kHz V^{-1}. We measured the resonance frequency continuously with a closed feedback loop using a lock-in-amplifier, PI controller, and a signal generator. Using the same procedure, we injected the fluorescent antibodies of higher concentrations, 40 and 80 μg ml^{-1}, in the next microchannel one at a time.

Depending on the concentrations of antibodies, we measured various amounts of resonance frequency shifts and their reaction kinetics, as illustrated in Fig. 6(a). The resonance frequency of the cantilever was gradually decreased to 4.0, 5.0, and 5.2 kHz for concentrations of antibody solution of 20, 40, and 80 μg ml^{-1} respectively. Moreover, the higher concentrations of antibodies reacted on the cantilever faster than the lower concentrations. The binding kinetics of each antibody solution was saturated within 30 min, 15 min, and 8 min in order of lower to higher concentrations. Moreover, the surface tension of antibody solutions of 20, 40, and 80 μg ml^{-1} were measured to be 71.0, 67.7, and 61.0 mN m^{-1} using a goniometer. We estimated that any resonance frequency shifts caused by surface tension variations were less than 0.27 kHz at the maximum.

We concurrently examined the attachment of antibodies on the cantilever using a fluorescent microscopic method that observed the fluorescent intensity under the same experimental conditions, such as the concentration of antibodies, flow rates, functionalization processes, and so on. We measured the fluorescent intensity on the surface of cantilever for one hour during attachment of antibodies on the cantilever. The intensity was recorded for one hour with a sampling ratio of 0.5 Hz using the

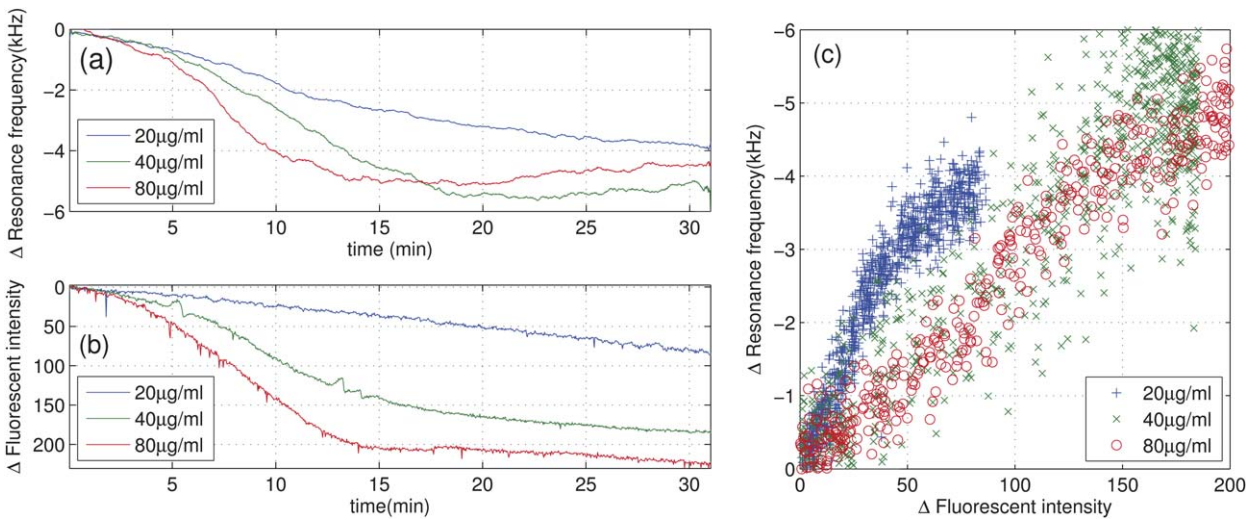

Fig. 6 Attachment of antibodies on the surface of the cantilever measured by the resonance frequency (a), and fluorescent intensity (b); (c) comparison between the resonance frequency shift and the fluorescent intensity change. Graph (b) shows a decreasing *y*-axis for ease of comparison. Note that the *y*-axes in graphs (b) and (c) are upside down.

fluorescent camera (Cascade II-512, Photometrics). The surface of the cantilever was observed using an objective lens of 20x through the PDMS cover and a 400 μm high microchannel using fluorescent excitation at 568 nm. Three microchannels were used to inject antibody solutions of 20 μg ml^{-1}, 40 μg ml^{-1}, and 80 μg ml^{-1} concentrations. The fluorescent intensity on the surface became brighter in all conditions. For the higher concentration of antibodies, the intensity increased faster and became brighter than for the lower concentration, as shown in Fig. 6(b).

We compared the two kinds of experimental methods for various concentrations in a graph to analyze the reaction kinetics. The reaction kinetics in both methods were correlated to each other, which shows that the shifts in the resonance frequency were caused by the peptide bonding of antibodies (Fig. 6(c)). Meanwhile, the reaction kinetics discerned by fluorescent observation were mostly slower than those observed with the resonance frequency measurement.

6. Conclusions

We developed a biosensor with a dynamic cantilever resonating at the air–liquid interface. The resonance properties of the cantilever were characterized as 62% larger vibrating amplitude, 50% higher quality factor, and 5.7 times higher signal-to-noise-ratio than the completely submerged cantilever; this corresponds to a 25-fold increase in frequency resolution over the cantilever in liquid. The micro-slit around the cantilever split the air–liquid phase at a meniscus membrane with elastic properties. We studied the effects of the meniscus membrane by varying the gap width of the micro-slit as well as by varying the surface tension using various levels of surfactant concentration. We found the slit width of 6 μm gave the best performance and also the surface tension ranging from 57 to 71 mN m^{-1} caused insignificant variation as compared with the resonance frequency changes by loaded mass. The feasibility of the cantilever-based biosensor was demonstrated by monitoring the covalent attachment of fluorescent antibodies with 20, 40, and 80 μg ml^{-1} concentrations. By comparing the results measured by resonance frequency shift and fluorescent intensity, we confirmed both methods showed good agreement.

Acknowledgements

This work was supported by the research project Development of a bio/nano-hybrid platform technology towards regenerative medicine (project leader: Prof. Hidetoshi Kotera), CREST in Japan Science and Technology Agency (JST). We gratefully acknowledge Prof. Masao Washizu, Prof. Dominique Collard, Prof. Beomjoon Kim, Dr. Laurent Jalabert and Dr. M. Catagay Tarhan for their valuable discussion about the research and Mr. Mauricio Cordero for critical reading of this paper. Moreover, one of authors, Jungwook Park, has been supported by G-COE program Secure-life Electronics of MEXT (Ministry of Education, Culture, Sports, Science and Technology).

References

1 G. Whiteside, *Nature*, 2006, **442**, 368–373.
2 J. El-Ali, P. K. Sorger and K. F. Jensen, *Nature*, 2006, **442**, 403–411.
3 H. Craighead, *Nature*, 2006, **442**, 387–393.
4 G. S. Fiorini and D. T. Chiu, *BioTechniques*, 2005, **38**, 429–446.
5 T. P. Burg, A. R. Mirza, N. Milovic, C. H. Tsau, G. A. Popescu, J. S. Foster and S. R. Manalis, *J. Microelectromech. Syst.*, 2006, **15**, 1466–1475.
6 K. Hwang, S. Lee, S. Kim, J. Lee and T. Kim, *Annu. Rev. Anal. Chem.*, 2009, **2**, 77–98.
7 N. Backmann, C. Zahnd, F. Huber, A. Bietsch, A. Pluckthun, H. P. Lang, H. J. Guntherodt, M. Hegner and C. Gerber, *Proc. Natl. Acad. Sci. U. S. A.*, 2005, **102**, 14587–14592.
8 G. Wu, R. H. Datar, K. M. Hansen, T. Thundat, R. J. Cote and A. Majumdar, *Nat. Biotechnol.*, 2001, **19**, 856–860.
9 J. Fritz, M. K. Baller, H. P. Lang, H. Rothuizen, P. Vettiger, E. Meyer, H.-J. Guntherodt, C. Gerber and J. K. Gimzewski, *Science*, 2000, **288**, 316–318.
10 K. Y. Gfeller, N. Nugaeva and M. Hegner, *Biosens. Bioelectron.*, 2005, **21**, 528–533.
11 K. Y. Gfeller, N. Nugaeva and M. Hegner, *Appl. Environ. Microbiol.*, 2005, **71**, 2626–2631.
12 S. Lee, K. Hwang, H. Yoon, D. Yoon, S. Kim, Y. Lee and T. Kim, *Lab Chip*, 2009, **9**, 2683–2690.
13 B. Cha, S. Lee, J. Park, K. Hwang, S. Kim, Y. Lee, B. Ju and T. Kim, *Biosens. Bioelectron.*, 2009, **25**, 130–135.
14 T. Kwon, K. Eom, J. Park, D. Yoon, H. Lee and T. Kim, *Appl. Phys. Lett.*, 2008, **93**, 173901.
15 K. Hwang, J. Lee, J. Park, D. Yoon, J. Park and T. Kim, *Lab Chip*, 2004, **4**, 547–552.
16 T. Braun, M. K. Ghatkesar, N. Backmann, W. Grange, P. Boulanger, L. Letellier, H.-P. Lang, A. Bietsch, C. Gerber and M. Hegner, *Nat. Nanotechnol.*, 2009, **4**, 179–185.
17 D. Jin, H. Bao, Z. Zhang, Y. Wang, H. Yu, G. Zuo and X. Li, *Appl. Phys. Lett.*, 2007, **90**, 041901.
18 X. Xia, Z. Zhang and X. Li, *J. Micromech. Microeng.*, 2008, **18**, 035028.
19 J. Lee, W. Shen, K. Payer, T. P. Burg and S. R. Manalis, *Nano Lett.*, 2010, **10**, 2537–2542.
20 T. P. Burg, M. Godin, S. M. Knudsen, W. Shen, G. Carlson, J. S. Foster, K. Babcock and S. R. Manalis, *Nature*, 2007, **446**, 1066–1069.
21 M. Godin, F. F. Delgado, S. Son, W. H. Grover, A. K. Bryan, A. Tzur, P. Jorgensen, K. Payer, A. D. Grossman, M. W. Kirschner and S. R. Manalis, *Nat. Methods*, 2010, **7**, 387–390.
22 J. Lee, R. Chunara, W. Shen, K. Payer, K. Babcock, T. P. Burgg and S. R. Manalis, *Lab Chip*, 2011, **11**, 645–651.
23 P. Dextras, T. P. Burg and S. R. Manalis, *Anal. Chem.*, 2009, **81**, 4517–4523.
24 M. G. von Muhlen, N. D. Brault, S. M. Knudsen, S. Jiang and S. R. Manalis, *Anal. Chem.*, 2010, **82**, 1905–1910.
25 S. Nishida, D. Kobayashi, Y. Nishimori and H. Kawakatsu, *J. Vac. Sci. Technol., B*, 2009, **27**, 964–968.
26 S. Nishida, D. Kobayashi, T. Sakurada, T. Nakazawa, Y. Hoshi and H. Kawakatsu, *Rev. Sci. Instrum.*, 2008, **79**, 123703.
27 H. Kawakatsu, S. Kawai, D. Saya, M. Nagashio, D. Kobayashi, H. Toshiyoshi and H. Fujita, *Rev. Sci. Instrum.*, 2002, **73**, 2317–2320.
28 P. Lambert, M. Mastrangeli, J. B. Valsamis and G. Degrez, *Microfluid. Nanofluid.*, 2010, **9**, 797–807.
29 H. Yuan, W. M. Mullett and J. Pawliszyn, *Analyst*, 2001, **126**, 1456–1461.